

Large modulation of the Shubnikov-de Haas oscillations by the Rashba interaction at the LaAlO₃/SrTiO₃ interface

A. Fête,¹ S. Gariglio,¹ C. Berthod,¹ D. Li,¹ D. Stornaiuolo,¹ M. Gabay,² and J.-M. Triscone¹

¹Department of Quantum Matter Physics, Université de Genève, 24 Quai Ernest-Ansermet, 1211 Genève 4, Suisse

²Laboratoire de Physique des Solides, Bat. 510, Université Paris-Sud 11, Centre d'Orsay, 91405 Orsay Cedex, France

We investigate the 2-dimensional Fermi surface of high-mobility LaAlO₃/SrTiO₃ interfaces using Shubnikov-de Haas oscillations. Our analysis of the oscillation pattern underscores the key role played by the Rashba spin-orbit interaction brought about by the breaking of inversion symmetry, as well as the dominant contribution of the heavy d_{xz}/d_{yz} orbitals on electrical transport. We furthermore bring into light the complex evolution of the oscillations with the carrier density, which is tuned by the field effect.

The conducting interface between the two band insulators LaAlO₃ (LAO) and SrTiO₃ (STO) has drawn a lot of attention as it presents a variety of exciting properties, among them superconductivity and a large spin-orbit coupling, both being tunable by an electric field [1]. As the 2DEG lies on the STO side, the conduction band of the system is dominated by the Ti 3d- t_{2g} orbitals as for bulk STO. However, at the interface quantum confinement spectacularly alters the orbital ordering of the energy levels, as observed by X-ray spectroscopy [2]: for a given sub-band index, the states with predominantly d_{xy} symmetry have, on average, a lower energy than states derived from the d_{xz}/d_{yz} orbitals. Currently, experimental and theoretical estimates of the out-of-plane extent of the 2DEG vary from a few monolayers [3–5] to 10 nm [6–8] and, consequently, the number and precise energy arrangement of these sub-bands is still an open question. The asymmetric confining potential also brings about a breaking of inversion symmetry: its effect is to spin-split the electronic bands (Rashba effect) [9–11] with important consequences on the magnetotransport of the system [12–14].

In this letter, we study the strength of the Rashba spin-orbit coupling in interfaces with low carrier densities ($\approx 10^{12} \text{ cm}^{-2}$). By analyzing the Shubnikov-de Haas (SdH) oscillations, we show that, the splitting induced by the Rashba spin-orbit interaction (SOi) is similar, in these samples, to the one observed in interfaces displaying higher carrier densities [12–14]. At these low-density interfaces, we find that the Fermi energy (E_F) is comparable to the spin-orbit splitting, defining an unusual regime when compared to semiconductor 2DEG. We contend that this situation makes the analysis of the quantum oscillations more subtle, due to the presence of two “pseudo-frequencies” related to the two spin-split level families. Electric field effect experiments reveal that the evolution of the Landau levels (LLs) that is observed as one changes the carrier density is singular.

The LaAlO₃ layers were grown by pulsed laser deposition at 650 °C, a lower temperature than for standard interfaces [15]. Hall bars for DC transport measurements were patterned and field-effect devices were realized using the STO single crystal substrate as the gate dielectric (see Supplemental Material [16]). Magnetotransport measurements were performed in a dilution refrigerator equipped with a

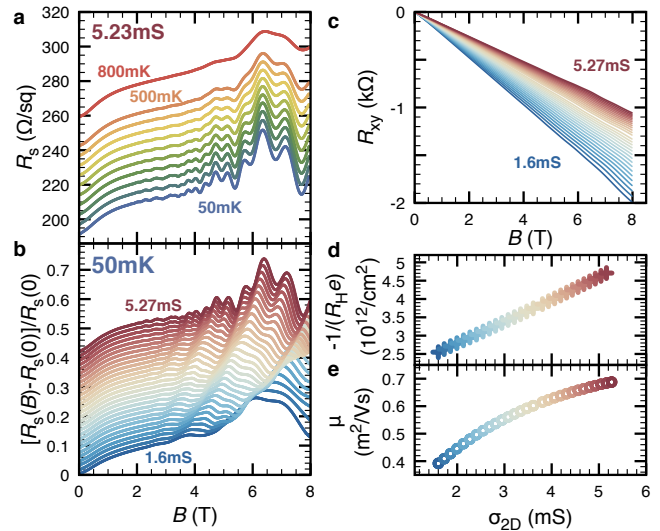


FIG. 1. Transport properties in a magnetic field. (a) Temperature evolution of the sheet resistance (R_s) versus magnetic field for a doping level corresponding to a sheet conductance of 5.23 mS and a mobility of $\mu \approx 7000 \text{ cm}^2\text{V}^{-1}\text{s}^{-1}$ at 50 mK. Curves are offset for clarity. In this paper, the sheet conductance at 50 mK and 0 T (σ_{2D}) is used as a reference for the doping level. (b) $[R_s(B) - R_s(0)]/R_s(0)$ for different dopings, illustrating the evolution of the SdH oscillations with gate voltage. Curves are offset for clarity. (c) Hall resistance versus magnetic field at 50 mK for different dopings. (d) Inverse Hall coefficient and (e) the corresponding Hall mobility at 50 mK versus σ_{2D} .

8 T superconducting magnet.

Figure 1a displays a set of sheet resistance versus magnetic field (B) curves for temperatures ranging from 800 mK to 50 mK. As can be seen, the magnitude of the Shubnikov-de Haas oscillations increases markedly as the temperature is lowered. At 50 mK and in high magnetic field, the amplitude of SdH oscillations is about 10–15% of the sheet resistance value. To change the carrier density, we apply a back-gate voltage [17]. Fig. 1c shows that upon carrier density tuning the transverse resistance R_{xy} varies linearly with magnetic field. From Fig. 1d, we see that ramping the gate voltage (V_g) up to large positive values leads to an increase of the inverse Hall coefficient. Analysing the Hall signal using a single-band model, we extract a carrier

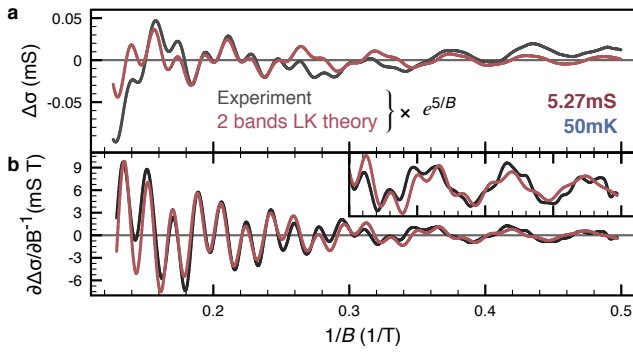


FIG. 2. (a) Comparison between $\Delta\sigma$ versus $1/B$ calculated within the two-band model (red) and the experimental data (black) for the doping with the highest conductance (5.27 mS) and at 50 mK. The exponential factor $e^{5/B}$ is used to magnify the low-field region. (b) Derivative with respect to B^{-1} of the curves presented in (a). (inset) Close-up on the low-field region of (b).

density at 50 mK that increases from 2.5 to $4.8 \times 10^{12} \text{ cm}^{-2}$ as V_g is swept from 79 to 107 V, *i.e.* as the sheet conductance (σ_{2D}) at 0 T increases from 1.6 to 5.27 mS.

Concomitantly with this variation of the electron density, the electron mobility μ evolves from 3900 to $6900 \text{ cm}^2\text{V}^{-1}\text{s}^{-1}$, as shown in Fig. 1e [14, 18, 19]. As can be seen in Fig. 1b, the changes in electron mobility and density strongly modify the structure of the SdH oscillations with a clear change in both the peak position and the period of the oscillations.

In order to proceed with the analysis of the SdH data presented in Fig. 1, we subtracted the background:

$$\Delta\sigma(B) = \frac{R_s(B)}{[R_s(B)]^2 + [R_{xy}(B)]^2} - \sigma_0(B) \quad (1)$$

with $R_s(B)$ and $R_{xy}(B)$ the measured longitudinal and transverse resistances, respectively, and $\sigma_0(B)$ a non-oscillating polynomial background. Examples of the resulting curves can be found in Fig. 4.

Looking at the SdH oscillations, we note (at least) two frequencies modulating the conductance. Hence, we first analyse the data considering a model with two parabolic bands for which the magnetoconductance can be calculated using the Lifshitz-Kosevich (LK) formula [20]. We fit the data for the largest conductance introducing an arbitrary phase for each frequency.

As can be seen from Fig. 2a, a good fit to the data can be obtained using the two frequencies 18 T and 55.9 T [4]. Panel b displays the derivatives of the theoretical and experimental curves allowing the positions of the maxima and minima to be compared. Considering the Onsager relation with a spin degeneracy of $\nu_s = 2$ and a valley degeneracy of $\nu_v = 1$, we find the carrier densities for the two bands to be 0.87 and $2.7 \times 10^{12} \text{ cm}^{-2}$, which yield a total carrier concentration of $\sim 3.6 \times 10^{12} \text{ cm}^{-2}$. This value is of the same order of magnitude as that extracted from

Hall effect measurements, albeit slightly lower. We note that similar discrepancies between the sheet carrier densities obtained using Hall effect data and SdH oscillations have already been reported [15, 22–24]. A possible explanation is that carriers with a lower mobility contribute to the Hall and magnetoresistance response, but not to the oscillations.

In the LK formalism, the temperature evolution of the oscillations has the following functional form:

$$\Delta\sigma_i(B_m, T) \propto \frac{\alpha_{LK,i} T}{\sinh(\alpha_{LK,i} T)} \quad (2)$$

with $\alpha_{LK,i} = 2\pi^2 k_B / \hbar \omega_{c,i}^*$, $\omega_{c,i}^* = eB_m / m_i^*$, B_m the field at which the extremum is observed, i the band index, T the temperature, and $-e$ the electronic charge.

We extracted the high and low frequency (HF and LF) parts of the SdH oscillations shown in Fig. 2a. Selecting 17 and 4 extrema for the HF and LF, respectively, good agreement between theory and experiment is obtained by choosing an effective mass of $2.7m_e$ for the HF and $1.25m_e$ for the LF (see Supplemental Material [16]). The value of the light mass is in line with previously reported estimates for STO based heterostructures [15, 22, 23]. Likewise, the presence and importance of carriers with a heavier mass have been recently revealed from the analyses of magneto-transport in perpendicular and parallel fields [14].

With the information extracted from this analysis, the electronic structure of our two-band model can be reconstructed and the splitting at the Fermi level between the heavy and the lighter bands determined:

$$\Delta E = |E_1(\bar{k}_F) - E_2(\bar{k}_F)|, E_i(k) = \frac{\hbar^2}{2m_i^*} (k^2 - k_{F,i}^2). \quad (3)$$

$k_{F,i}$ is the Fermi momentum in the i -th band obtained from the area $A_i = \pi k_{F,i}^2$ calculated using the Onsager relation, and $\bar{k}_F = (k_{F,1} + k_{F,2})/2$. We find $\Delta E \approx 2.45 \text{ meV}$.

Remarkably, the calculated band splitting ΔE is similar to the typical Rashba spin-orbit splitting estimated for LAO/STO heterostructures [12, 13]. In a Rashba scenario, the SOi splits the LLs of a single band into two families (\pm) of irregularly-spaced levels. These energy levels are labeled by an integer $N \geq 0$ and read, for an isotropic Fermi surface and a k -linear splitting [26]:

$$E_{N=0} = E_c/2 - E_Z, E_{N>0}^{\pm} = NE_c \mp \sqrt{(E_c/2 - E_Z)^2 + NE_c^2}. \quad (4)$$

$E_c = \hbar\omega_c^*$, $E_Z = (g^*/2)\mu_B B$ is the Zeeman splitting, $E_\alpha = \alpha\sqrt{2eB/\hbar}$ with α the Rashba coupling constant. The $N = 0$ state is fully spin-polarized, and the two series of LLs with $N > 0$ correspond to orthogonal mixtures of spin-up and spin-down states.

To compare the data with this second model, we computed numerically the DOS, the chemical potential, and the conductance for each magnetic field and temperature, using the formalism of Ref. 2. We considered a Gaussian

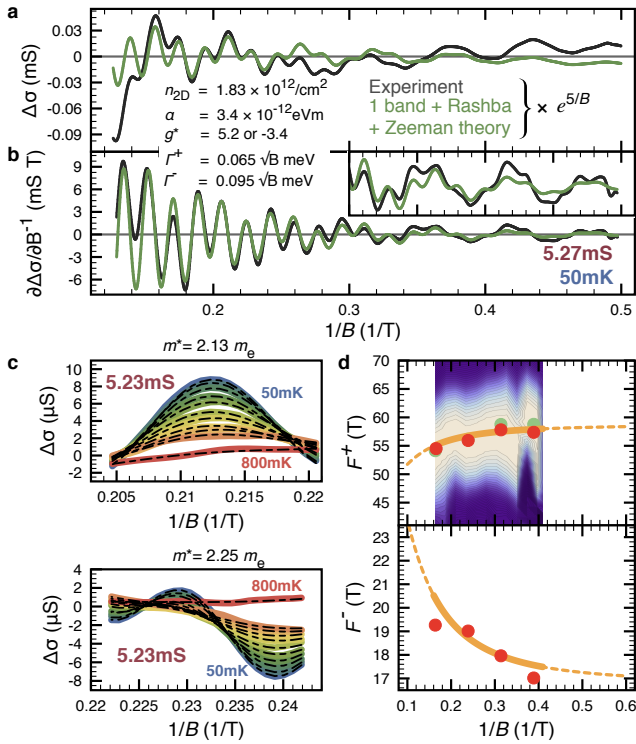


FIG. 3. (a) Comparison between $\Delta\sigma$ measured experimentally for $\sigma_{2D} = 5.27$ mS (black) and calculated using our single-band model with Rashba and Zeeman interactions (green). (b) Derivative with respect to B^{-1} of the curves presented in (a). The exponential factor $e^{5/B}$ is used to magnify the low-field region. (inset) Close-up on the low-field region of (b). (c) Temperature dependence of the oscillations over the two ranges of applied field used to extract the effective mass. Black dashed lines are the theoretical curves computed using $m^* \sim 2.2m_e$, while the thick coloured lines are the experimental data. (d) Magnetic field dependence of F^+ (top) and F^- (bottom). Red and green dots correspond, respectively, to the estimation made via the band pass filtered and differentiated signals. The background is a color plot based on the short time Fourier Transform of $\Delta\sigma$.

broadening of the LLs with a variance $\gamma \pm \sqrt{B}$. The results are displayed in Fig. 3. As can be seen, good agreement between the data and the theory is obtained (see Supplemental Material [16]).

The carrier density extracted from this analysis is $n_{2D}^{\text{SdH}} = 1.83 \times 10^{12} \text{ cm}^{-2}$, substantially lower than the one found using the Hall effect measurements. As discussed for the two-band model, this is not surprising, as only bands with a mobility larger than $\approx 2000 \text{ cm}^2\text{V}^{-1}\text{s}^{-1}$ will give rise to observable SdH oscillations at the relatively low fields used here. The magnitude of the obtained Rashba coupling constant ($\alpha = 3.4 \times 10^{-12} \text{ eV m}$) agrees very well with values obtained from weak localization analyses and from modelling of the transport data in parallel fields [12–14]. We note that, given the small value of k_F in our samples, a k -cubic Rashba interaction inducing a spin-splitting of $\approx 2 \text{ meV}$ would require a very large coupling constant α_3 ,

beyond the values recently reported by H. Nakamura *et al.* [29].

To obtain the effective mass, we selected three peaks from a region of magnetic fields where the amplitude of the oscillations is large. Fig. 3c shows that the data can be fit perfectly using an effective mass of $2.19 \pm 0.06m_e$. This value may indicate that the electronic state of the oscillating carriers is not dominated by Ti d_{xy} orbitals, as one would then expect a lower effective mass ($\sim m_e$). Instead, the higher mass obtained in this analysis can be understood by taking into account the contribution of d_{xz}/d_{yz} orbitals to the electronic states. We note that a recent analysis of photoemission spectra for interfaces grown at 650°C , complemented by *ab initio* calculations, was consistent with a 2DEG having occupied d_{xz}/d_{yz} electronic states at the Fermi energy [30].

This observation corroborates our recent results on standard LAO/STO interfaces, where a sharp decrease in the elastic scattering rate was correlated to the progressive appearance, at the Fermi level, of heavier carriers [14]. The average effective mass of the carriers was observed to evolve from $\sim 0.7m_e$ to $\sim 2.2m_e$, $2.2m_e$ being precisely the value observed here. These results appear to showcase the critical role played by heavier carriers in establishing high-mobility at the LAO/STO interface. We note that this feature gives further substance to a scenario of spin-orbit protected transport due to a Fermi surface reconstruction induced by the Rashba interaction [14].

Because the Zeeman energy enters equation (5) only as a squared term, for the LLs with $N > 0$, we find two solutions for the g^* -factor, namely 5.2 or -3.4 , values similar to the ones observed in semiconductor heterostructures. We note that g^* -factors significantly different from 2 where predicted by *ab initio* calculations in bulk STO [31]. In this second scenario, we can also estimate the Rashba splitting and the Fermi energy. Interestingly, we find that both are of the same order of magnitude: $\Delta_R = 2.2 \text{ meV}$ and $E_F = 1.65 \text{ meV}$, a situation very different from the one of many semiconductor 2DEGs, where the Fermi energy dominates.

The physical pictures emerging from the two previous analyses seem quite different. Can we understand the results obtained using the LK formula in the light of the band structure suggested by the Rashba model? In the particular regime that we are studying, it can be shown (see Supplemental Material [16]) that two “pseudo-frequencies” (F^+ and F^-) can be observed for, respectively, the evolution in magnetic field of the “+” and “-” LLs located close to the Fermi level. In addition to that, these two components of the quantum oscillations have different temperature behaviors, which, if analyzed using the LK formula, lead to two different effective masses (m_+^* and m_-^*). Interestingly enough, theory predicts that m_+^* is always larger than m_-^* . Using the parameters of the fit presented in Fig. 3 yields $F^- = 19.5 \text{ T}$, $F^+ = 56 \text{ T}$, $m_-^* = 1.6m_e$ and $m_+^* = 2.8m_e$ (at $B = 5 \text{ T}$, see below). These values are in line with our first analysis.

Owing to the complexity of the Rashba LLs spectrum, F^- ,

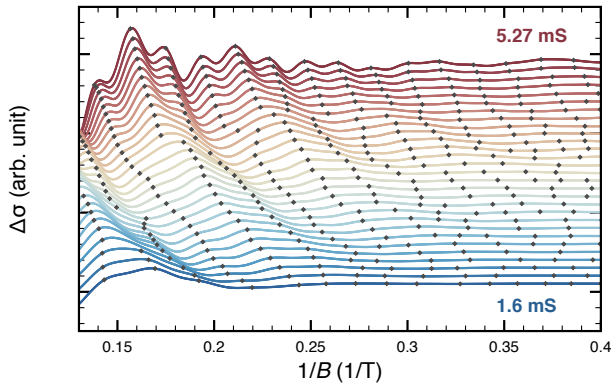


FIG. 4. Analysis of the doping dependence of the SdH oscillations. Curves are shifted for clarity. Black dots indicate the position where maxima occur in $-\Delta\sigma''(1/B)$.

F^+ , m_-^* and m_+^* are all magnetic field dependent. While the variations of m_+^* and m_-^* with B are below our experimental resolution, such is not the case for the variations of F^- and F^+ . We have estimated, from the data, F^- and F^+ as a function of magnetic field using three different procedures (see Supplemental Material [16]). Fig. 3d shows the estimated F^- and F^+ as a function of $1/B$ on top of the theoretical prediction (thick orange line). A very good agreement is obtained both in the amplitudes and in the signs of the frequency variations. We note that the field dependence of F^- and F^+ is probably the reason why the low field region of the quantum oscillations is fitted better by the Rashba model than by the two-band model (compare plots in inset of Fig. 2b and Fig. 3b).

In a 2DEG with more than one sub-band populated, inter-sub-band scattering was shown to bring additional components to the Shubnikov-de Haas oscillations [32, 33]. More recently, this effect was also discussed for systems composed of a unique Rashba spin-orbit split band [6]: the (pseudo-)frequencies associated to this phenomenon are $F^+ + F^-$ and $F^+ - F^-$. Looking at the Fourier transform of our data (see Supplemental Material [16]), we indeed observe maxima in the spectrum of the oscillations located at $F^+ + F^-$ and $F^+ - F^-$.

We finally discuss the gate-voltage dependence of the SdH oscillations. Fig. 4 shows the change in conductance as a function of $1/B$ for various V_g (*i.e.* σ_{2D}). A clear evolution of the SdH oscillations with decreasing doping is visible and is compatible with the shrinking of the Fermi surface expected from Hall measurements. With the help of the second derivative $-\Delta\sigma''(1/B) = -\partial^2\Delta\sigma/\partial(1/B)^2$ which amplifies F^+ , we identify all maxima from the “+” levels as a function of applied applied gate voltage. These maxima are indicated in Fig. 4 by black dots. We expect that the trajectories traced out by the black dots as a function of V_g correspond to the evolution of each LL as a function of the chemical potential. Strikingly, we see that these trajectories present sharp deviations or jumps upon decreasing

V_g . This feature is clearly visible on a fan diagram featuring $-\Delta\sigma''(1/B)$ versus (B, σ_{2D}) (see Supplemental Material [16]) which nicely illustrates the fact that the position of the “+” LLs follows a simple evolution only for limited regions of the diagram. Conversely, we observe that at precise locations the amplitude of the SdH oscillations is strongly suppressed.

There are many situations in which quantum oscillations rapidly change their phase and/or amplitude as a function of B . An example is the exchange interaction that enhances the g^* -factor for magnetic fields beyond a critical value [35–42]. Changes in the oscillation pattern can also occur when different LLs cross at a particular magnetic field: in this case anti-crossings can be observed [43–49]. These phenomena originate from many-body interactions. The deviations observed in Fig. 4 point to an interaction whose energy scale is of the order of the LL splitting (≈ 0.1 meV at 2.5 T for the highest doping and the “+” levels). Further studies are needed to determine the nature of this interaction.

The study presented here unravels the remarkably complex behavior of the Shubnikov-de Haas oscillations seen at the LAO/STO interface. Our analysis reveals the important role played by the Rashba SOI on the electronic band structure and the peculiar regime hereby realized. Finally, the evolution of the LL spectrum as a function of doping and magnetic field displays sharp deviations that we cannot explain in our independent electron picture.

The authors would like to thank G. Seyfarth and D. Jaccard for help with the measurements and stimulating discussions, and are grateful to M. Lopes and S. C. Müller for their technical assistance. This work was supported by the Swiss National Science Foundation through the NCCR MaNEP and Division II, by the Institut Universitaire de France (MG) and has received funding from the European Research Council under the European Union’s Seventh Framework Programme (FP7/2007-2013) / ERC Grant Agreement n^o 319286.

-
- [1] P. Zubko, S. Gariglio, M. Gabay, P. Ghosez, and J.-M. Triscone, *Annu. Rev. Cond. Mat. Phys.* **2**, 141 (2011).
 - [2] M. Salluzzo, J. C. Cezar, N. B. Brookes, V. Bisogni, G. M. De Luca, C. Richter, S. Thiel, J. Mannhart, M. Huijben, A. Brinkman, G. Rijnders, and G. Ghiringhelli, *Phys. Rev. Lett.* **102**, 166804 (2009).
 - [3] M. Sing, G. Berner, K. Goß, A. Müller, A. Ruff, A. Wetscherek, S. Thiel, J. Mannhart, S. A. Pauli, C. W. Schneider, P. R. Willmott, M. Gorgoi, F. Schäfers, and R. Claessen, *Phys. Rev. Lett.* **102**, 176805 (2009).
 - [4] C. Cancellieri, M. L. Reinle-Schmitt, M. Kobayashi, V. N. Strocov, T. Schmitt, P. R. Willmott, S. Gariglio, and J.-M. Triscone, *Phys. Rev. Lett.* **110**, 137601 (2013).
 - [5] P. Delugas, A. Filippetti, V. Fiorentini, D. I. Bilc, D. Fontaine, and P. Ghosez, *Phys. Rev. Lett.* **106**, 166807 (2011).
 - [6] N. Reyren, S. Gariglio, A. D. Caviglia, D. Jaccard, T. Schneider, and J.-M. Triscone, *Appl. Phys. Lett.* **94**, 112506 (2009).

- [7] O. Copie, V. Garcia, C. Bödefeld, C. Carrétéro, M. Bibes, G. Herranz, E. Jacquet, J.-L. Maurice, B. Vinter, S. Fusil, K. Bouzouhane, H. Jaffrès, and A. Barthélémy, *Phys. Rev. Lett.* **102**, 216804 (2009).
- [8] G. Khalsa and A. H. MacDonald, *Phys. Rev. B* **86**, 125121 (2012).
- [9] Z. Zhong, A. Tóth, and K. Held, *Phys. Rev. B* **87**, 161102 (2013).
- [10] Y. Kim, R. M. Lutchyn, and C. Nayak, *Phys. Rev. B* **87**, 245121 (2013).
- [11] G. Khalsa, B. Lee, and A. H. MacDonald, *Phys. Rev. B* **88**, 041302 (2013).
- [12] A. D. Caviglia, M. Gabay, S. Gariglio, N. Reyren, C. Cancellieri, and J.-M. Triscone, *Phys. Rev. Lett.* **104**, 126803 (2010).
- [13] M. Ben Shalom, M. Sachs, D. Rakhmilevitch, A. Palevski, and Y. Dagan, *Phys. Rev. Lett.* **104**, 126802 (2010).
- [14] A. Fête, S. Gariglio, A. D. Caviglia, J.-M. Triscone, and M. Gabay, *Phys. Rev. B* **86**, 201105 (2012).
- [15] A. D. Caviglia, S. Gariglio, C. Cancellieri, B. Sacépé, A. Fête, N. Reyren, M. Gabay, A. F. Morpurgo, and J.-M. Triscone, *Phys. Rev. Lett.* **105**, 236802 (2010).
- [16] See Supplemental Material at ... for details on thin film growth, patterning and fabrication of field effect devices and details on the analysis of quantum oscillations.
- [17] In the rest of the paper we use the sheet conductance at zero magnetic field and 50 mK (σ_{2D}) rather than the gate voltage (V_g) to define the state of the system as σ_{2D} is more convenient to compare results from different runs.
- [18] C. Bell, S. Harashima, Y. Kozuka, M. Kim, B. G. Kim, Y. Hikita, and H. Y. Hwang, *Phys. Rev. Lett.* **103**, 226802 (2009).
- [19] A. Joshua, S. Pecker, J. Ruhman, E. Altman, and S. Ilani, *Nature Comm.* **3**, 1129 (2012).
- [20] I. M. Lifshitz and A. M. Kosevich, *Zh. Eksp. Teor. Fiz.* **29**, 730 (1955), [*Sov. Phys. JETP* **2**, 636 (1956)].
- [4] We would like to emphasize that at our base temperature ($k_B T \approx 10^{-3}$ meV) the field dependence of the amplitude of the oscillations is mainly controlled by the Dingle term that compares the strength of the disorder to the cyclotron gap. Hence, the fitting shown in Fig. 2b is only sensitive to the product of m^* and the Dingle temperature.
- [22] Y. Kozuka, M. Kim, C. Bell, B. G. Kim, Y. Hikita, and H. Y. Hwang, *Nature* **462**, 487 (2009).
- [23] B. Jalan, S. Stemmer, S. Mack, and S. J. Allen, *Phys. Rev. B* **82**, 081103 (2010).
- [24] M. Ben Shalom, A. Ron, A. Palevski, and Y. Dagan, *Phys. Rev. Lett.* **105**, 206401 (2010).
- [25] I. A. Luk'yanchuk and Y. Kopelevich, *Phys. Rev. Lett.* **93**, 166402 (2004).
- [26] R. Winkler, *Spin-orbit Coupling Effects in Two-Dimensional Electron and Hole Systems* (Springer, Berlin, 2003).
- [2] T. Ando and Y. Uemura, *J. Phys. Soc. Jpn.* **36**, 959 (1974).
- [28] Y. M. Zhou, G. Yu, T. Lin, N. Dai, and J. H. Chu, *Physica B: Cond. Mat.* **407**, 116 (2012).
- [29] H. Nakamura, T. Koga, and T. Kimura, *Phys. Rev. Lett.* **108**, 206601 (2012).
- [30] C. Cancellieri, M. L. Reinle-Schmitt, M. Kobayashi, V. N. Strocov, P. R. Willmott, D. Fontaine, Ph. Ghosez, A. Filippetti, P. Delugas and V. Fiorentini, *Phys. Rev. B* **89**, 121412 (2014).
- [31] D. van der Marel, J. L. M. van Mechelen, and I. I. Mazin, *Phys. Rev. B* **84**, 205111 (2011).
- [32] P. T. Coleridge, *Semicond. Sci. Technol.* **5**, 961 (1990).
- [33] D. R. Leadley, R. Fletcher, R. J. Nicholas, F. Tao, C. T. Foxon, and J. J. Harris, *Phys. Rev. B* **46**, 12439 (1992).
- [6] S. Novokshonov, *Low Temp. Phys.* **39**, 378 (2013).
- [35] J. Janak, *Phys. Rev.* **178**, 1416 (1969).
- [36] R. Nicholas, R. Haug, K. Klitzing and G. Weimann, *Phys. Rev. B* **37**, 1294 (1988).
- [37] M. M. Fogler and B. I. Shklovskii, *Phys. Rev. B* **52**, 17366 (1995).
- [38] D. R. Leadley, R. J. Nicholas, J. J. Harris and C. T. Foxon, *Phys. Rev. B* **58**, 13036 (1998).
- [39] S. Brosig, K. Ensslin, A. G. Jansen, C. Nguyen, B. Brar, M. Thomas, and H. Kroemer, *Phys. Rev. B* **61**, 13045 (2000).
- [40] B. A. Piot, D. K. Maude, M. Henini, Z. R. Wasilewski, K. J. Friedland, R. Hey, K. H. Ploog, A. I. Toropov, R. Airey and G. Hill, *Phys. Rev. B* **72**, 245325 (2005).
- [41] C. H. Yang and W. Xu, *J. Appl. Phys.* **103**, 013707 (2008).
- [42] S. S. Krishnopenko, K. P. Kalinin, V. I. Gavrilenko, Yu. G. Sado-fyev, and M. Goiran, *Semiconductors* **46**, 1163 (2012).
- [43] K. Muraki, T. Saku, and Y. Hirayama, *Phys. Rev. Lett.* **87**, 196801 (2001).
- [44] X. C. Zhang, D. R. Faulhaber, and H. W. Jiang, *Phys. Rev. Lett.* **95**, 216801 (2005).
- [45] X. C. Zhang, I. Martin, and H. W. Jiang, *Phys. Rev. B* **74**, 073301 (2006).
- [46] C. Ellenberger, B. Simovič, R. Leturcq, T. Ihn, S. E. Ulloa, K. Ensslin, D. C. Driscoll, and A. C. Gossard, *Phys. Rev. B* **74**, 195313 (2006).
- [47] G. Yu, D. J. Lockwood, A. J. SpringThorpe, and D. G. Austing, *Phys. Rev. B* **76**, 085331 (2007).
- [48] T. Jungwirth and A. H. MacDonald, *Phys. Rev. B* **63**, 035305 (2000).
- [49] P. M. Smith and M. P. Kennett, *J. Phys.: Cond. Mat.* **24**, 055601 (2012).

Large modulation of the Shubnikov-de Haas oscillations by the Rashba interaction at the LaAlO₃/SrTiO₃ interface - Supplemental Material

S1 – Growth conditions and sample geometry

LaAlO₃/SrTiO₃ interfaces were realized by growing 9 unit cells of LaAlO₃ on a (001) oriented TiO₂ terminated SrTiO₃ substrate using pulsed laser deposition. The deposition conditions were an oxygen pressure of 10⁻⁴ mbar, a substrate temperature of 650 °C, a repetition rate of the ablating laser of 1 Hz, and a fluence of 0.6 Jcm⁻². The growth process was monitored *in-situ* using reflection high energy electron diffraction (RHEED). After growth, the sample was annealed for 1 hour in 0.2 bar of O₂ at a temperature of ~ 530°C.

In order to avoid any photolithographic step after the layer deposition, we patterned the substrate with amorphous SrTiO₃ [1]. The dimensions of the Hall bars for magnetotransport measurements were 500μm × 1000μm (width×length). The field-effect devices were realized using the STO substrate as the gate dielectric adding a metallic contact on its backside (yellow rectangle, see Fig. 1). The blue arrow indicates the direction of the external magnetic field for all the magnetotransport measurements of this work.

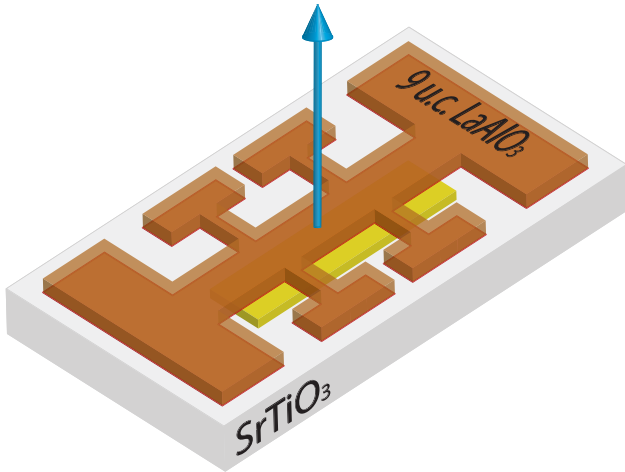


FIG. 1. Schematic view of sample geometry.

S2 – Effective mass associated with the high- and low-frequency components of the SdH oscillations

Figure 2 illustrates the procedure that we followed to extract the effective mass using Eq. (2) of the main text. The top (bottom) panel shows data obtained for the high-frequency (low-frequency) component of the magnetoconductance recorded at $\sigma_{2D} = 5.27$ mS. Each color is linked to the temperature evolution of a single oscillation.

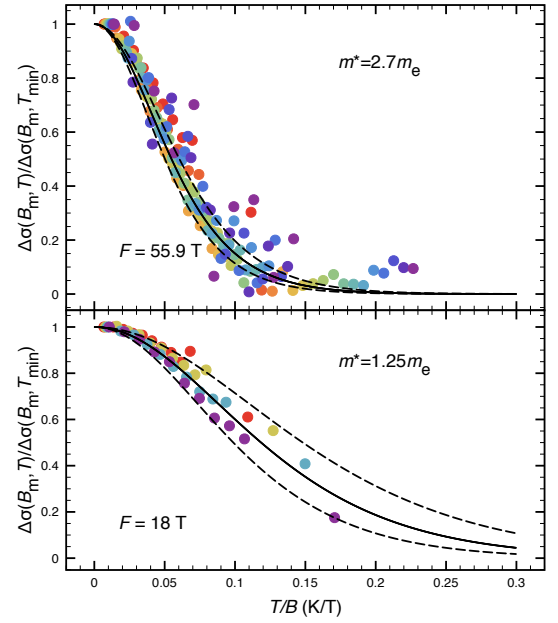


FIG. 2. Extraction of the effective mass from the temperature dependence of the Shubnikov-de Haas oscillations. Full lines correspond to the theoretical predictions taking m^* as effective mass. Dashed lines correspond to the theoretical predictions taking $m^* \pm 0.25m_e$.

S3 – Modeling the SdH oscillations in the case of a single band with Rashba/Zeeman splitting

In order to determine the SdH oscillations pattern of the conductance for a single band with Rashba and Zeeman splittings, we start with the expression of the Landau levels presented in the main text,

$$\begin{aligned} E_{N=0} &= E_c/2 - E_Z \\ E_{N>0}^{\pm} &= NE_c \mp \sqrt{(E_c/2 - E_Z)^2 + NE_{\alpha}^2}, \end{aligned} \quad (5)$$

with $E_c = \hbar\omega_c^*$, $E_Z = (g^*/2)\mu_B B$ the Zeeman splitting, and $E_{\alpha} = \alpha\sqrt{2eB/\hbar}$ with α the Rashba coupling. Setting the values of m^* , g^* , α , and B defines the energy of the Landau levels (LLs) for a given magnetic field (vertical red/blue lines in Fig. 3, top). We broaden each level using a gaussian line shape with a variance $\Gamma^{\pm} = \gamma^{\pm}\sqrt{B}$, and perform the sum over all levels to obtain the density of states $g(E)$:

$$g(E) = \frac{eB}{2\pi\hbar} \sum_{N,s=\pm} \frac{1}{\sqrt{2\pi}\Gamma^s} \exp\left[-\frac{1}{2}\left(\frac{E - E_N^s}{\Gamma^s}\right)^2\right]. \quad (6)$$

The result is shown in Fig. 3, bottom.

The chemical potential μ (vertical green line in Fig. 3) is obtained by solving numerically the equation giving the carrier concentration at a given temperature,

$$n_{2D} = \int_{-\infty}^{\infty} dE f(E - \mu)g(E), \quad (7)$$

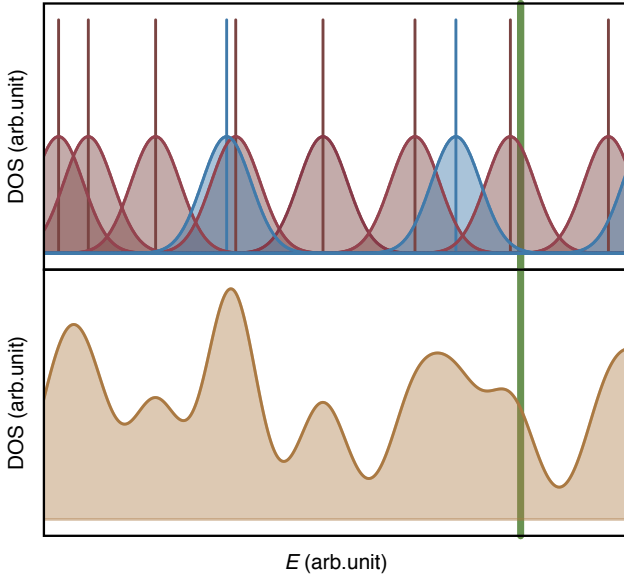


FIG. 3. (Top) Schematic view of the DOS for the two families (+, red; -, blue) of LLs in the Rashba model. (Bottom) Total DOS resulting from the sum of the + and - DOS. The green vertical line is the position of the Fermi level.

with $f(E) = (e^{E/k_B T} + 1)^{-1}$ the Fermi-Dirac distribution. Finally, the conductance is obtained via [2]:

$$\sigma_{xx} = \frac{e^2}{2\pi\hbar} \int_{-\infty}^{\infty} dE \left(-\frac{\partial f(E - \mu)}{\partial E} \right) \times \sum_{N,s=\pm} \left(N + \frac{1}{2} \right) \exp \left[-\left(\frac{E - E_N^s}{\Gamma^s} \right)^2 \right]. \quad (8)$$

We performed this calculation at each B in order to get the field dependence $\sigma_{xx}(B)$. Finally, the oscillating part $\Delta\sigma_{xx}(B)$ of the conductance was obtained by subtracting a curve computed using a sufficiently high temperature T_{high} , at which the SdH oscillations are completely suppressed:

$$\Delta\sigma_{xx}(B, T) = \sigma_{xx}(B, T) - \sigma_{xx}(B, T_{\text{high}}). \quad (9)$$

This method was successfully applied, e.g., in Ref. 3.

S4 – Minimal parametrization of the Landau-level spectrum in the case of a Rashba/Zeeman split system

In the presence of a linear Rashba spin-orbit interaction and a Zeeman splitting, the LLs spectrum of a parabolic and isotropic band is given by Eq. (5). Introducing the energy scale $E_{c,1} \doteq E_c(B = 1 \text{ T})$ to normalize the energies, $\tilde{E} = E/E_{c,1}$, Eq. (5) can be simplified:

$$\tilde{E}_0 = \frac{E_c}{2E_{c,1}} - \frac{E_Z}{E_{c,1}} = \frac{B}{2} \left(1 - \frac{g^* m^*}{2m_e} \right) \doteq \frac{Ba}{2} \quad (10)$$

with $a = 1 - g^* m^*/(2m_e)$. Similarly,

$$\begin{aligned} \tilde{E}_N^\pm &= N \frac{E_c}{E_{c,1}} \mp \sqrt{\left(\frac{E_c}{2E_{c,1}} - \frac{E_Z}{E_{c,1}} \right)^2 + N \frac{E_\alpha^2}{E_{c,1}^2}} \\ &= NB \mp \sqrt{\left(\frac{Ba}{2} \right)^2 + N \frac{2(am^*)^2}{e\hbar^3} \frac{1}{B}} \\ &= B \left(N \mp \frac{1}{2} \sqrt{a^2 + N \frac{D}{B}} \right) \end{aligned} \quad (11)$$

with $D = 8(am^*)^2/(e\hbar^3)$. We observe that, in the constant E_F approximation, only three parameters are required in order to determine the values B^* where the conductance is maximal [4]: those are \tilde{E}_F , a and D .

S5 – Using the LK formula to analyze the quantum oscillations in Rashba spin-orbit split bands

In this section we show that the LL spectrum generated by the Rashba spin-orbit model can be analyzed using the Lifshitz-Kosevich (LK) formula. In this case we obtain two effective masses and two “quasi-frequencies”. These additional calculations allow us to connect the two band analysis and the numerical simulation including Rashba SO interaction.

One important feature of the LK formula is that it assumes a LLs spectrum going as:

$$E_n = \hbar\omega_c^* \left(n + \frac{1}{2} \right) = \hbar \frac{eB}{m^*} \left(n + \frac{1}{2} \right) \quad (12)$$

Hence, in this model, the energy splitting between neighboring Landau levels is directly linked to the value of the effective mass and is independent of n . Indeed:

$$\frac{dE_n}{dn} = \hbar \frac{eB}{m^*} \quad (13)$$

For the Rashba spectrum Eq. (11), we get a very different result:

$$\frac{dE_{N>0}^\pm}{dN} = \hbar \frac{eB}{m^*} \left(1 \mp \frac{D}{4B} \frac{1}{\sqrt{a^2 + N \frac{D}{B}}} \right) \quad (14)$$

In this case, the splitting between LLs is N -dependent.

As we consider the conductance which is related to the DOS at the Fermi level, this spacing can be considered as almost constant for large N . More generally, we calculate, at a given magnetic field, the LL index at the Fermi level (N_F^\pm). Using the constant E_F approximation and restricting ourselves to $E_F \geq 0$ we get:

$$N_F^\pm = \frac{m^* E_F}{\hbar e B} + \frac{D}{8B} \pm \frac{\kappa}{8} \quad (15)$$

with:

$$\kappa = \sqrt{16a^2 + \frac{D}{B^2} \left(D + 16 \frac{m^* E_F}{\hbar e} \right)} \quad (16)$$

In turn, Eq. (15) can be used to define two “pseudo-frequencies” via:

$$F^\pm(1/B) = \frac{dN_F^\pm}{d(1/B)} \quad (17)$$

We get:

$$F^\pm(1/B) = \frac{m^* E_F}{e\hbar} + \frac{D}{8} \pm \left(\frac{\kappa}{8} - \frac{2a^2}{\kappa} \right) B \quad (18)$$

We observe that $F^+(1/B)$ and $F^-(1/B)$ depend on the magnetic field strength; this is the reason why we call them “pseudo-frequencies”. This dependence is due to the non-linear spacing of the Rashba/Zeeman split LLs. $F^+(1/B)$ is a decreasing function of B while $F^-(1/B)$ is an increasing function of B . As shown in the main text, even though this magnetic field dependence is weak, it can be evidenced in our experimental oscillations.

For the experimental determination of F^+ as a function of $1/B$ we used two techniques. The first one consists in using filtering techniques or the second derivative of $\Delta\sigma$ to isolate the oscillations associated to F^+ (red and green dots in Fig. 4a of the main text), dividing the field range in 4 regions of equal size in $1/B$ and fitting the oscillations (in each region) with a cosine of constant frequency. The second one is to compute the short time Fourier transform (FT) of $\Delta\sigma$ (color plot in Fig. 4a of the main text). For F^- , due to the limited number of oscillations, we could only apply the first technique.

Coming back to Eq. (14), the splitting between LLs at the Fermi level in a Rashba/Zeeman scenario is obtained by inserting Eq. (15) into Eq. (14):

$$\left(\frac{dE_{N>0}^\pm}{dN} \right)_{E=E_F} = \hbar \frac{eB}{m^*} \left(1 \mp D \frac{1}{B\kappa \pm D} \right) \quad (19)$$

which, if we define

$$m_\pm^* = m^* \left(1 \pm \frac{D}{B\kappa} \right) \quad (20)$$

can be rewritten in the same form as Eq. (13):

$$\left(\frac{dE_{N>0}^\pm}{dN} \right)_{E=E_F} = \hbar \frac{eB}{m_\pm^*} \quad (21)$$

Hence, in a magnetotransport experiment, if m_\pm^* does not vary too much with magnetic field, a Rashba/Zeeman split LLs spectrum can be interpreted as two independent series of LLs of the form given by Eq. (12) (*i.e.* an analysis of the quantum oscillations using the LK formula will not fail altogether). However, in this case, the effective mass associated

with $F^+(1/B)$ is larger than the effective mass associated with $F^-(1/B)$. This is exactly what we find.

We note that, with the parameters extracted from the fit shown in Fig. 3 of the main text, we find that the dependence of m_\pm^* on magnetic field is only of 5–10% between 2 and 8 T, which is below our experimental resolution.

Formula similar to the ones found in this section can be found in Ref. 5.

S6 – Determination of the effective masses associated with the quantum oscillations stemming from inter-sub-band scattering

According to theory the two components related to the inter-sub-band scattering have a different temperature behavior; a higher effective mass is associated to the one at $F^+ + F^-$ than to the one at $F^+ - F^-$.

In Fig. 4, we present an analysis of the temperature dependence of the oscillations associated with the maxima of the FT located at $F^+ + F^-$ and $F^+ - F^-$, for the measurement at the doping with the highest conductance (5.27 mS). We used band pass filters (whose limits are illustrated in Fig. 4) to select the different components of our spectrum. We obtain an effective mass of $1.75m_e$ and $2.5m_e$ for the component at $F^+ - F^-$ and $F^+ + F^-$, respectively. Due to the weak contribution of these frequencies to the total FT a non-negligible weight from the neighboring peaks is probably biasing our estimations.

Using the formula in [6], and the parameters of the fit presented in Fig. 3 of the main text, we calculate a mass of $\approx 1.2m_e$ (at $B = 5$ T) for the peak at $F^+ - F^-$, in reasonable agreement with our result.

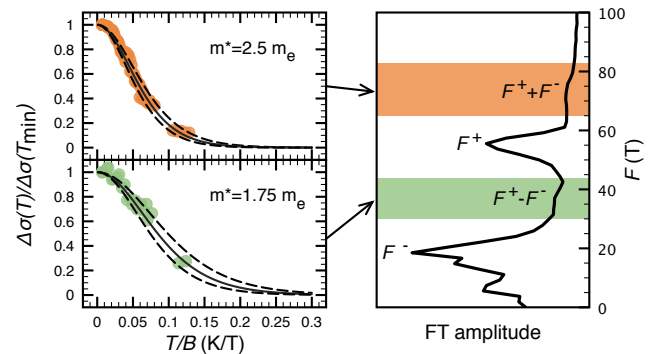


FIG. 4. (Left) Temperature dependence of the FT components located at $F^+ - F^-$ and $F^+ + F^-$, for the measurement at the doping with the highest conductance (5.27 mS). Full lines correspond to the theoretical predictions taking m^* as effective mass. Dashed lines correspond to the theoretical predictions taking $m^* \pm 0.25m_e$. (Right) Fourier transform of the same measurement. Colored regions define the limits of the band-pass filters.

**S7 – Evidence of a perturbed pattern of oscillations below
 ≈ 4.5 mS**

Figure 5 displays a fan diagram showing $-\Delta\sigma''(1/B)$. This nicely illustrates the fact that the position of the “+” LLs follows a simple evolution only for limited regions of the diagram. Conversely, we observe that at precise locations the amplitude of the SdH oscillations is strongly suppressed.

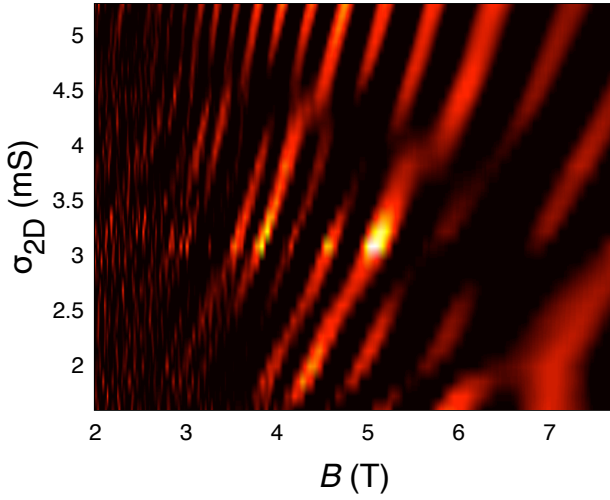


FIG. 5. Analysis of the doping dependence of the SdH oscillations. Fan diagram showing $-\Delta\sigma''(1/B)$; yellow corresponds to the maxima and black to negative values.

-
- [1] D. Stornaiuolo, S. Gariglio, N. J. G. Couto, A. Fête, A. D. Caviglia, G. Seyfarth, D. Jaccard, A. F. Morpurgo, and J.-M. Triscone, *Appl. Phys. Lett.* **101**, 222601 (2012).
 - [2] T. Ando and Y. Uemura, *J. Phys. Soc. Jpn.* **36**, 959 (1974).
 - [3] J. Luo, H. Munekata, F. F. Fang, and P. J. Stiles, *Phys. Rev. B* **41**, 7685 (1990).
 - [4] Maxima in the conductance arise when a Landau level is at the Fermi energy, i.e., when B is such that one of the equations (10) or (11) is verified with $\tilde{E} = \tilde{E}_F$.
 - [5] S. Novokshonov, and A. Groshev, *Phys. Rev. B* **74**, 245333 (2006).
 - [6] S. Novokshonov, *Low Temp. Phys.* **39**, 378 (2013).